Supplementary Information and Supplemental figures for

A multi-omics spatiotemporal atlas of the silkworm *(Bombyx mori)* wing disk and a gene transition model reveal 20-hydroxyecdysone-driven development reprogramming

Qingsong Liu[1, #], Mingmin He[2, #], Hao Chen[1, #], Yongfen Zhang[2, #], Wanshun Li[1, 3, 4, #], Xue Zhang[2], Xiaoyang Wang[1], Hongyan Li[2], Hongni Li[1], Dongsheng Ran[2], Zhangchen Tang[1], Yanan Wu[2], Lin Zhu[1], Xingju Zhang[2], Guoli Li[1], Longxing Wang[2, 5], Xiangyu Cai[1], Jian He[4], Xiao Liu[1], Feng Xi[2], Linshengzhe Ji[1], Guibo Li[2], Ying Lin[1], Guocheng Liu[4], Lingyan Wang[1], Xun Xu[3], Ping Zhao[1, *], Ao Chen[2, *], Min Xie[2, *], Qingyou Xia[1, *]

[1]Integrative Science Center of Germplasm Creation in Western China (CHONGQING) Science City, Biological Science Research Center, Southwest University, Chongqing 400715, China.

[2]BGI Research, Chongqing 401329, China.

[3]BGI Research, Shenzhen 518083, China.

[4]MGI Tech, Shenzhen 518083, China.

[5]School of Life Health Information Science and Engineering, Chongqing University of Posts and Telecommunication, Chongqing 400065, China.

[#]These authors contributed equally to the work.

[*]Corresponding Author: xiaqy@swu.edu.cn; xiemin@genomics.cn; chenao@genomics.cn; zhaop@swu.edu.cn.

Supplementary methods

20-hydroxyecdysone (20E) geneset

To identify the 20E hormone-related genes in silkworm wing discs (WDs), we conducted a comprehensive review ofrelevant literature available on the Web of Science[1-23]. Based on their functions and roles within signaling pathways, these genes were classified into several categories: 20E Receptor, 20E Signaling Cascade Proteins, Signal Cascade-Related Enzymes, Immune-Related Factors, Functional Proteins, Protein Receptors, Transcription Factors (TFs), and Cuticular Proteins. A detailed list of these genes is provided in Table S4. This classification offers a systematic framework for understanding the roles of these genes in WD development and their involvement in the 20E signaling network.

Drosophila melanogaster WD single-cell RNA sequencing (scRNA-seq) data analysis

Sequencing data and aligned matrixes were downloaded from the GEO database (accession code GSE155543). The standard analysis pipeline was the same as that used in the article methods[24]. Clusters were split into AMP and epithelial cells. Finally, we obtained 12,872 cells and 6,552 homologous features with the silkworm. Correlations were calculated using Spearman's method.

Supplemental Figures

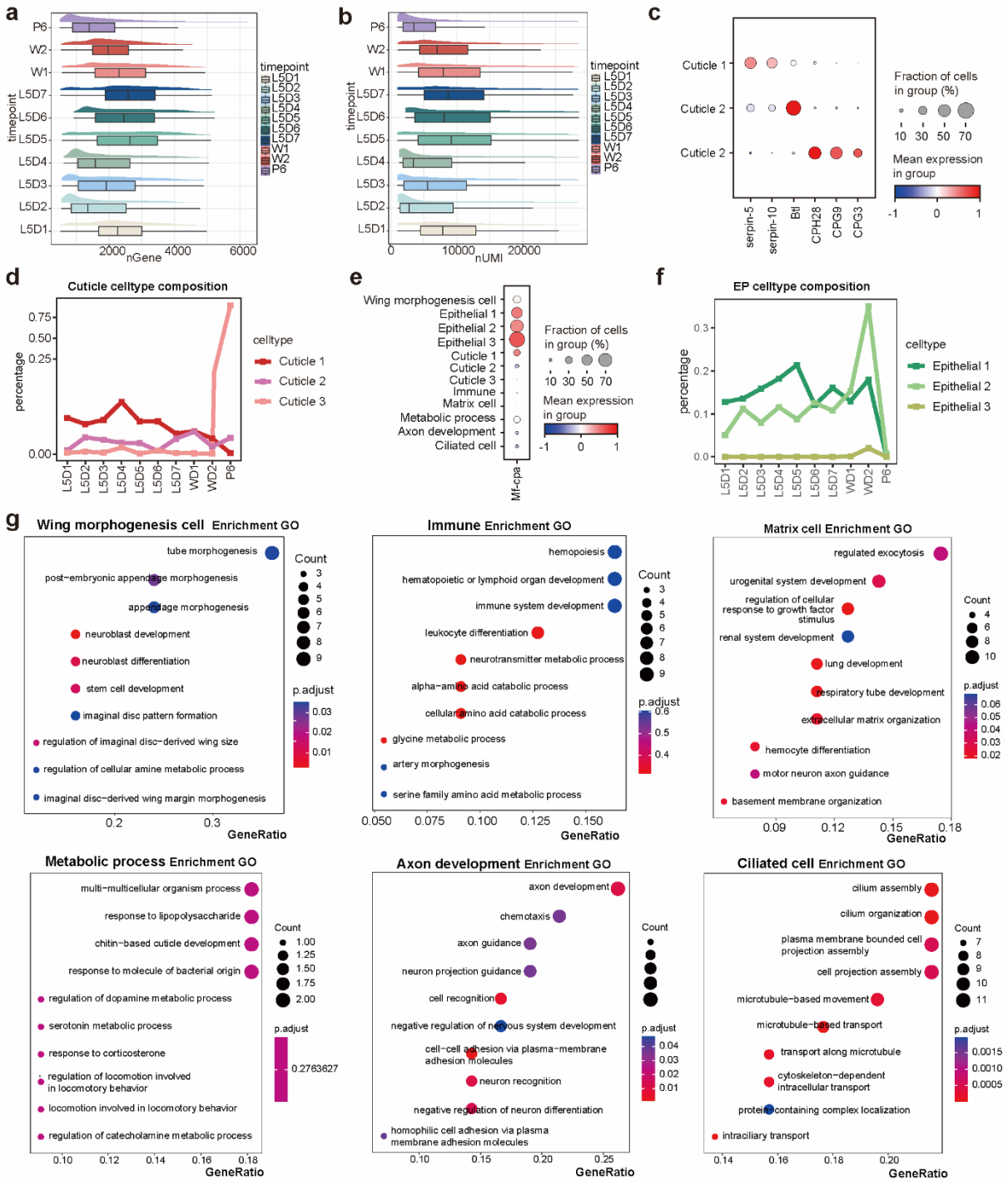

Supplementary Fig. 1. Foundational scRNA-seq transcriptomics data of *Bombyx mori* WD development.

a. Distribution of the number of detected genes per cell (nGenes) across different developmental time points.

b. Distribution of the number of unique molecular identifiers (nUMIs) across developmental stages.

c. Dot plot showing the enrichment of marker genes specific to Cuticle cell subtypes.

d. Temporal changes in the proportions of Cuticle cell subtypes (Cuticle 1, Cuticle 2, Cuticle 3) across all stages.

e. Dot plot showing the enrichment of marker genes specific to Epithelial cell subtypes.

f. Temporal changes in the proportions of Epithelial cell subtypes (Epithelial 1, 2, 3) during development.

g. Gene Ontology (GO) enrichment analysis of six cell types (Wing morphogenesis cell, Immune, Apoptosis, Metabolic, Axon development, and Ciliated cell).

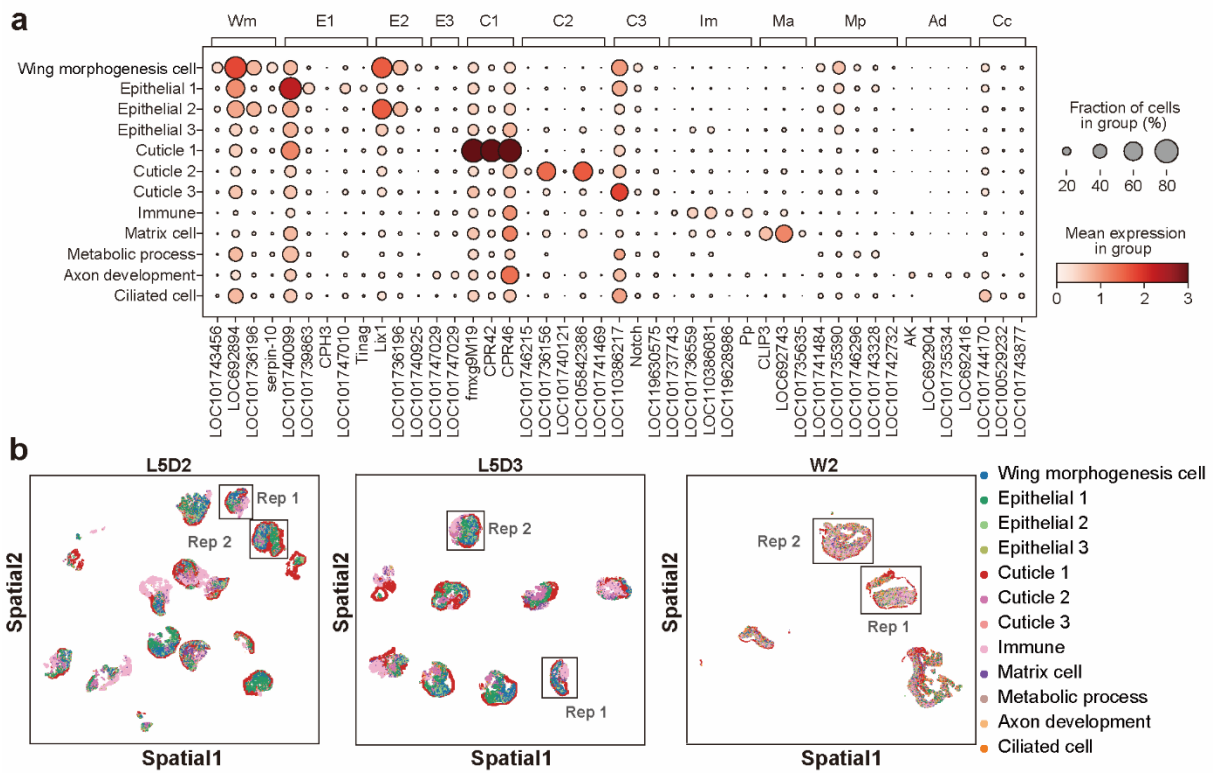

Supplementary Fig. 2. Spatiotemporal transcriptomic data supporting cell type identification and localization.

a. Spatiotemporal omics-annotated cell type deconvolution marker gene heatmap.

b. Spatial distribution of annotated cell types in wing discs at three developmental time points (L5D2, L5D3, and W2) based on spatiotemporal transcriptomic data. Regions with relatively intact wing disc morphology are boxed and displayed in the main figure panels.

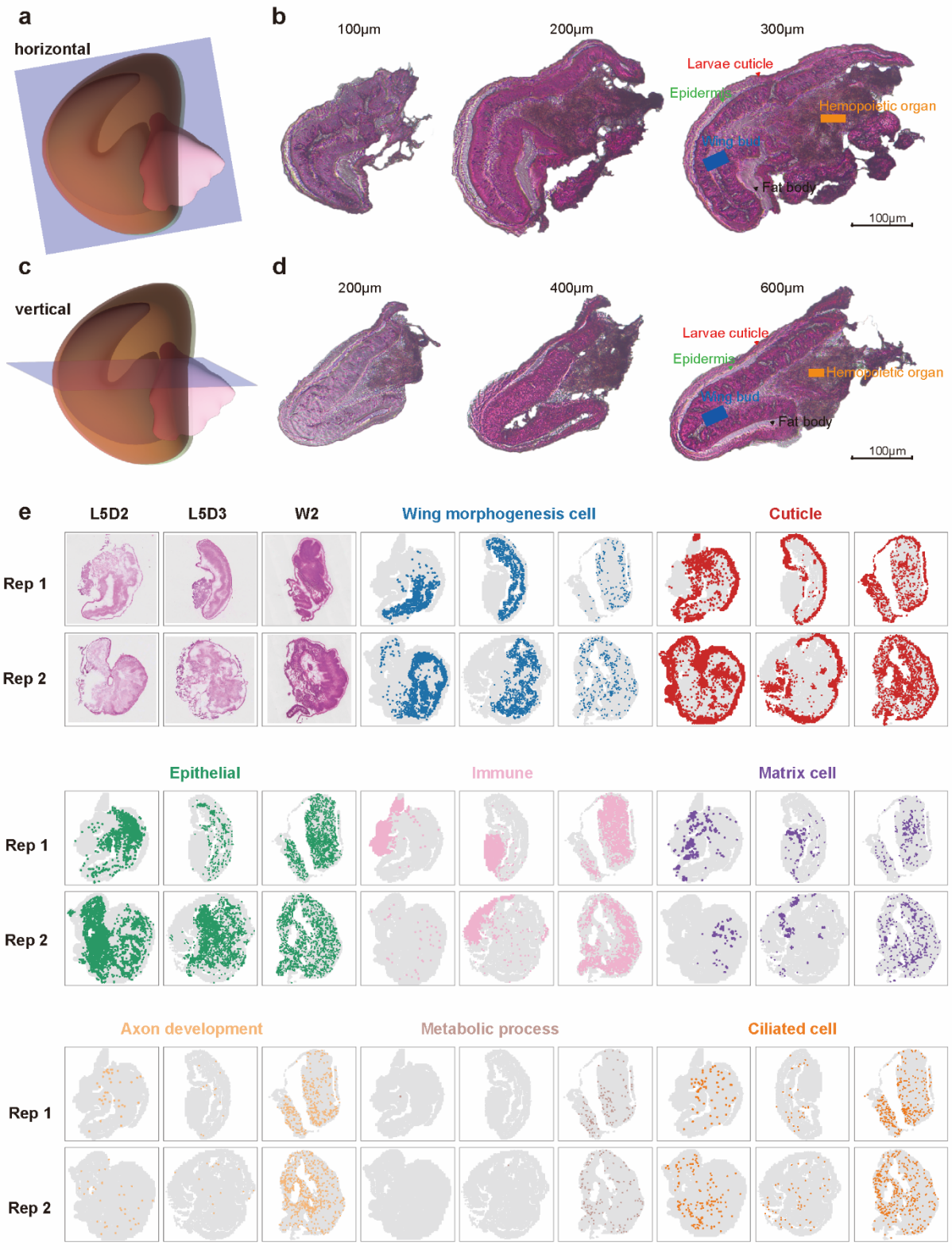

Supplementary Fig. 3. Histological architecture and spatial localization of cell types within the wing disc.

a. Schematic diagram illustrating the anatomical structure of the wing disc and its horizontal

cross-section.

b. Hematoxylin and eosin (HE) staining of horizontal sections of the wing disc at increasing tissue depths (100, 200, and 300 μm). Major structures including the larval cuticle, epidermis, wing sac, wing cavity, hemopoietic organ, and fat body are annotated.

c. Schematic diagram of the wing disc with a longitudinal (vertical) sectioning orientation..

d. HE staining of longitudinal sections at different depths (200, 400, and 600 μm), highlighting key internal structures.

e. Histological sections of wing discs at three developmental stages (L5D2, L5D3, and W2) with corresponding spatial transcriptomics data showing *in situ* distribution of annotated cell types. Two biological replicates are shown per stage. Cell types include Wing morphogenesis, Cuticle, Epithelial, Immune, Apoptosis, Axon development, Metabolic process, and Ciliated cells.

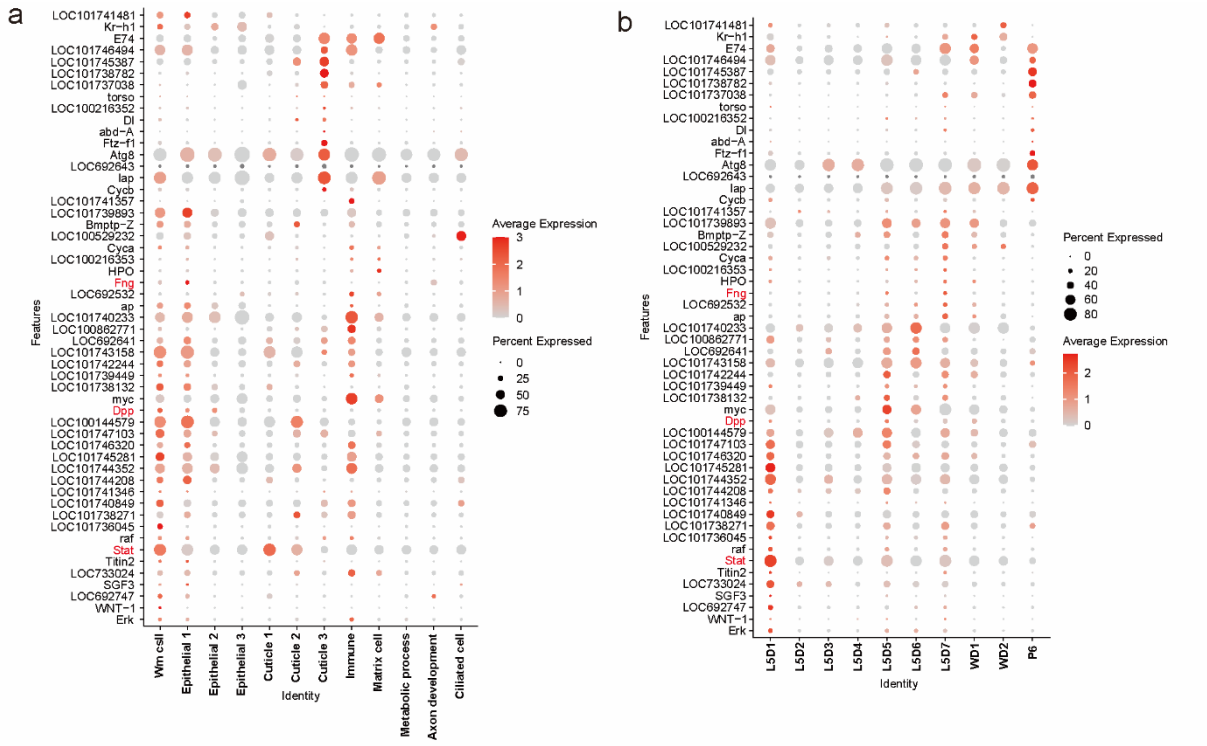

81

82 **Supplementary Fig. 4. Expression patterns of known developmental regulators across**
83 **cell types, time points, and spatial transcriptomic slices.**

84 **a**. Dot plot showing the expression of previously reported developmental genes across all
85 annotated cell types in the wing disc.

86 **b**. Expression dynamics of the same gene set across 10 developmental time points, from
87 L5D1 to P6.

88

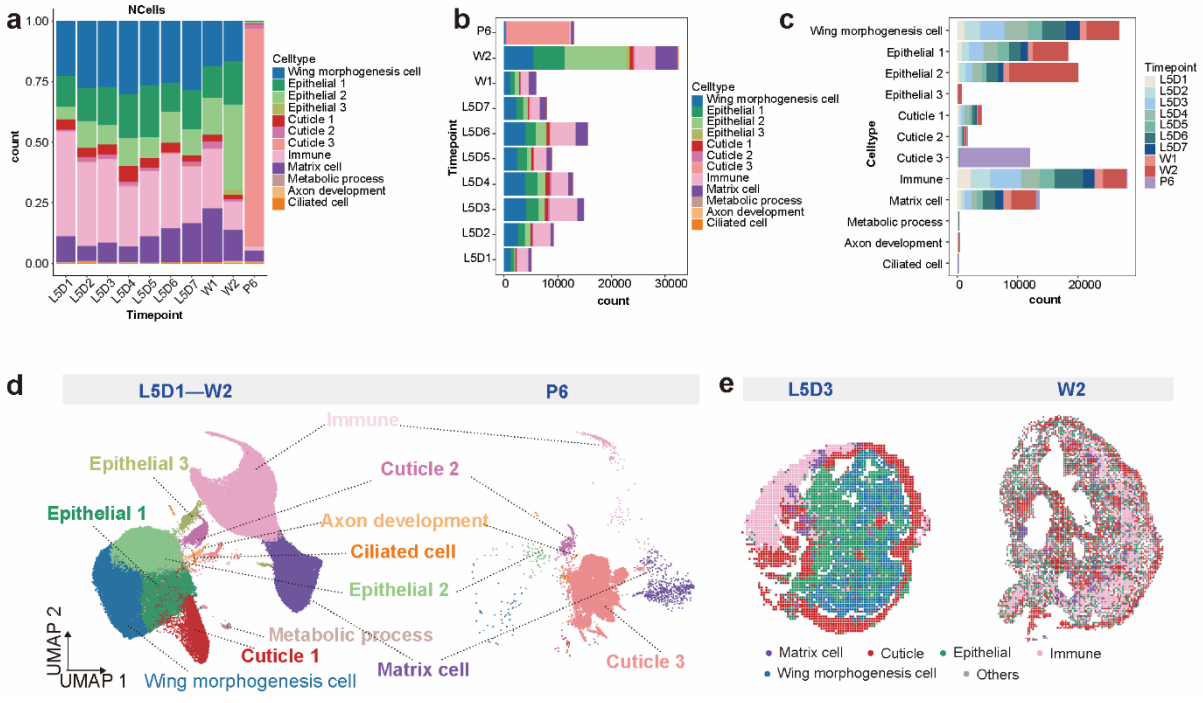

Supplementary Fig. 5. Distribution and dynamics of cell types across developmental stages.

a. Quantitative changes in cell numbers across different developmental stages (L5D1–P6).

b. Proportion and absolute cell counts of different cell types identified across the 10 developmental time points.

c. Total number and temporal distribution of annotated cell types, represented as proportions of total dissociated cells at each developmental stage.

d. UMAP visualization of cell clusters from L5D1 to W2 and P6 stages, with distinct cell types labeled.

e. Spatial transcriptomic maps showing the localization of major cell types in wing discs at L5D3 and W2. Each color represents a different annotated cell type.

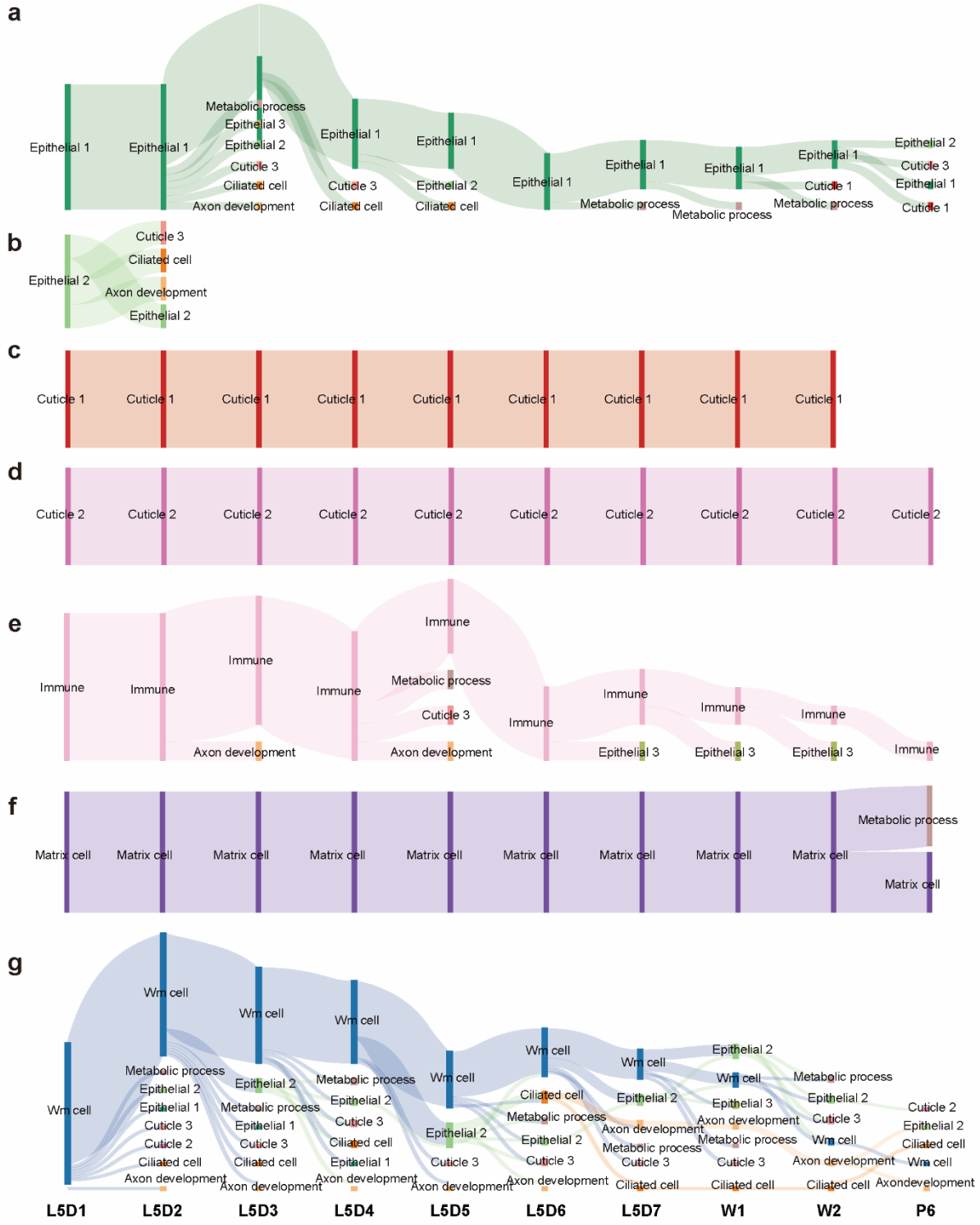

Supplementary Fig. 6. TOME-tradj analysis reveals developmental trajectories of individual cell types during wing disc maturation.

a. Epithelial 1 primarily undergoes differentiation and development centered on epithelial cells.

b. Epithelial 2 ceases differentiation after a certain period.

c. Cuticle 1 develops based on the original cell type.

d. Cuticle 2 develops based on the original cell type.

e. Immune cells develop based on the original cell type, with their numbers gradually decreasing throughout the developmental process.

f. Matrix cells develop based on the original cell type.

g. The differentiation trajectory of wing morphogenesis (Wm) cells progresses toward other differentiation types.

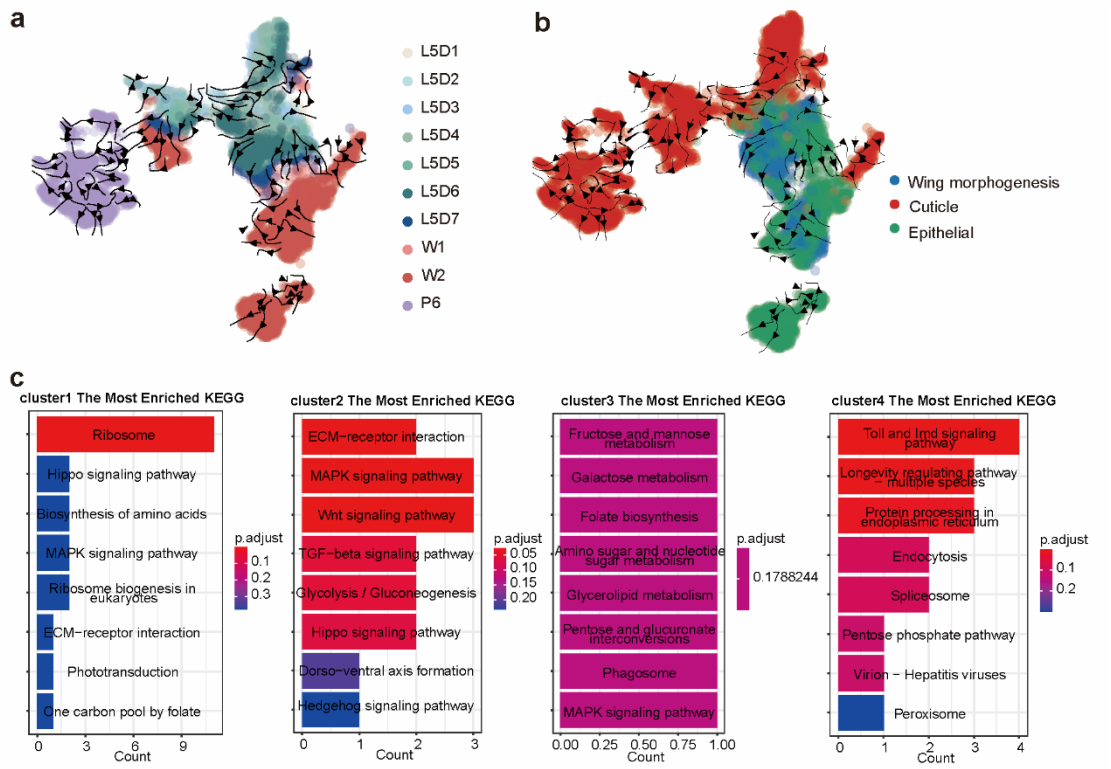

Supplementary Fig. 7. Enrichment clustering and differentiation trajectories of Wm cells in spatiotemporal transcriptomic sections.

a. The differentiation trajectory of Wm cells in different development stages.

b. Wm cells differentiate into Cuticle and Epithelial types.

c. KEGG pathway enrichment analysis revealed the functional enrichment of different clusters of Wm cells during differentiation.

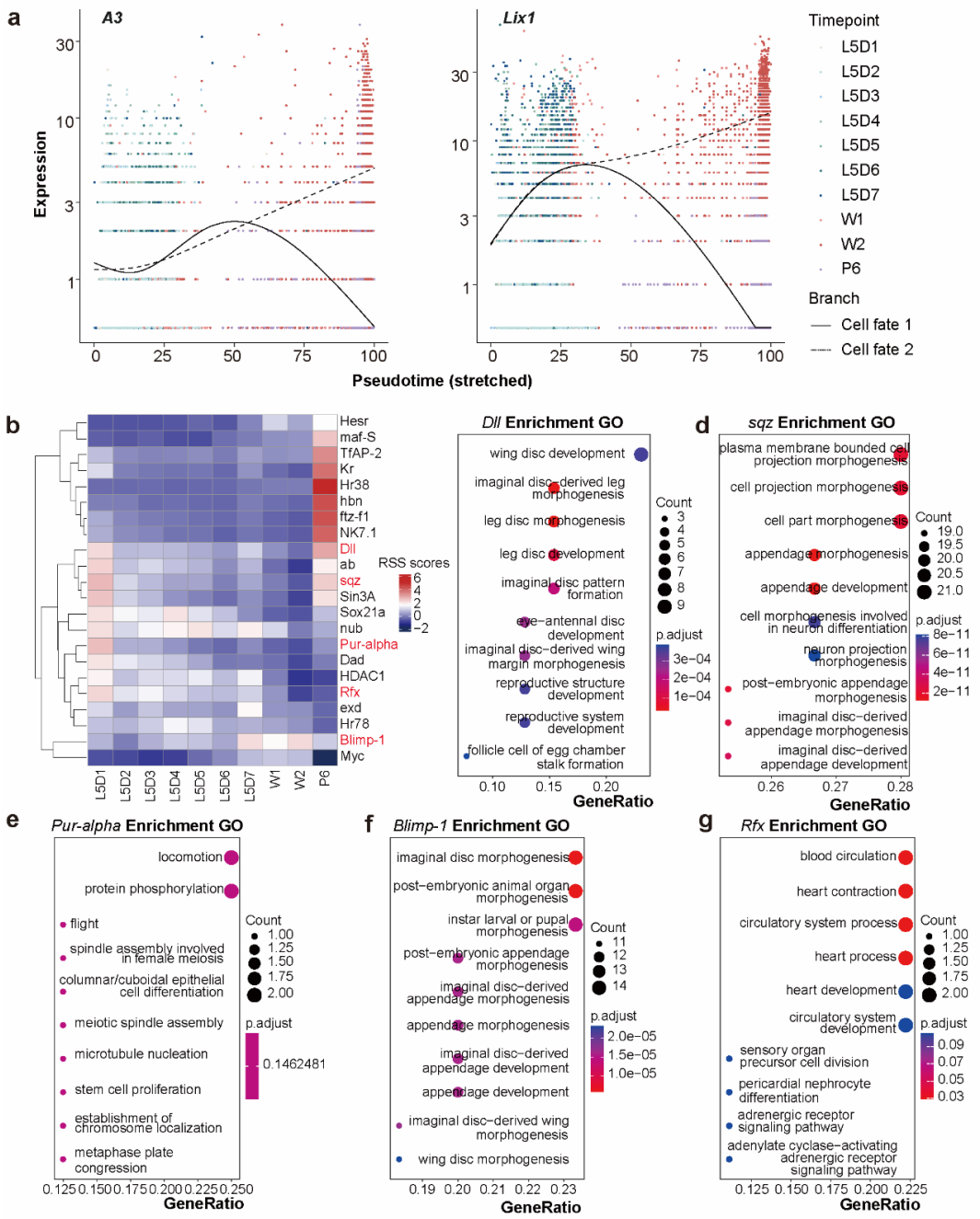

Supplementary Fig. 8. Functional enrichment of gene clusters and transcription factors associated with Wm cell differentiation.

a. The expression patterns of Hippo pathway genes in cell fate (*A3* and *Lix1*).

b. Heatmap of regulon specificity scores (RSS) of transcription factors (TFs) in Wm cells, which displays the transcription activity of various TFs in different stages of the wing disc cells.

c–**g**. GO enrichment analyses of the top five TFs (*Dll*, *sqz*, *Pur-alpha*, *Blimp-1*, and *Rfx*) identified in Wm cells.

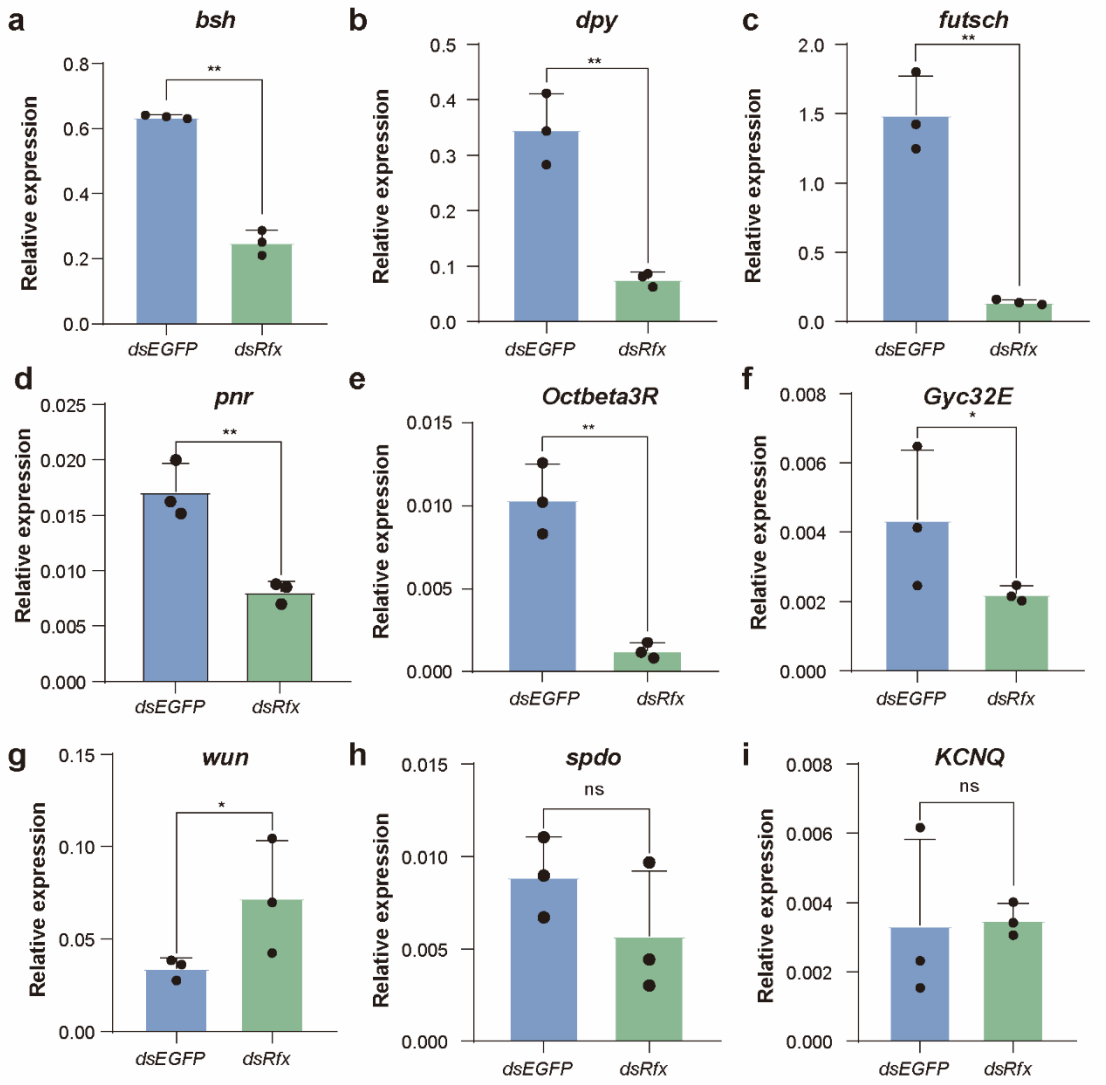

Supplementary Fig. 9. Quantitative analysis of *Rfx*-associated downstream gene expression.

a–**i.** qRT-PCR analysis of nine genes—*bsh*, *dpy*, *futsch*, *pnr*, *Octbeta3R*, *Gyc32E*, *wun*, *spdo*, and *KCNQ*—after *Rfx* knockdown. Data represented by the mean ± SD were analyzed for intergroup comparison using unpaired *t*-tests, with significance at *, $p < 0.05$, **, $p < 0.01$, ns = not significant.

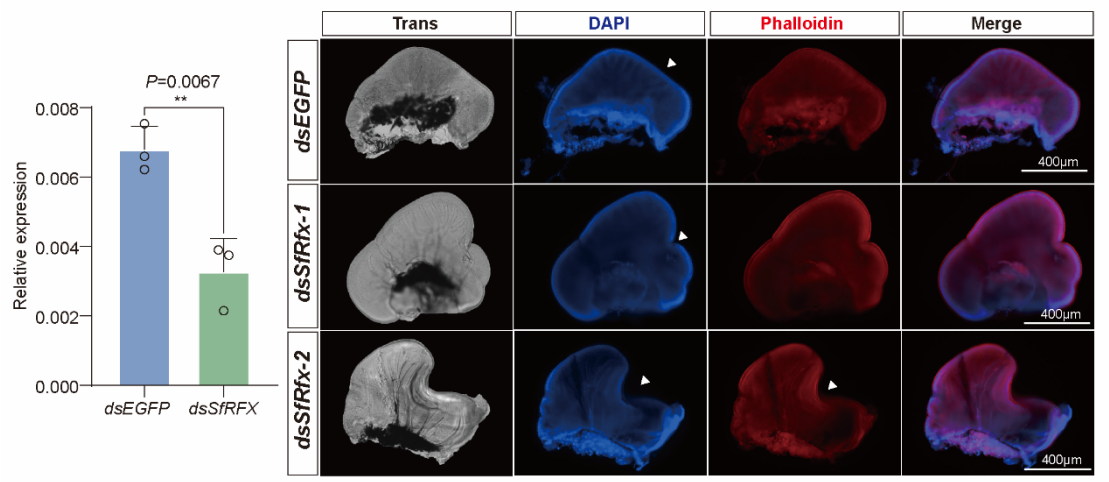

Supplementary Fig. 10. Effect of *SfRfx* gene knockdown on wing development in the fall armyworm *Spodoptera frugiperda*.

a. qPCR analysis of gene changes after *SfRfx* gene interference, Data represented by the mean ± SD, were analyzed for intergroup comparison using unpaired *t*-tests, with significance at **, $p < 0.01$.

b. Morphological changes in wing discs of fall armyworm after *SfRfx* gene knockdown, showing developmental fissures and defects. Bright-field imaging revealed the overall tissue architecture. Phalloidin staining labeled actin filaments to visualize cytoskeletal organization. DAPI staining marked nuclear DNA for cellular localization. Merged images integrated Phalloidin and DAPI signals to delineate spatial relationships between cytoskeletal elements and nuclei.

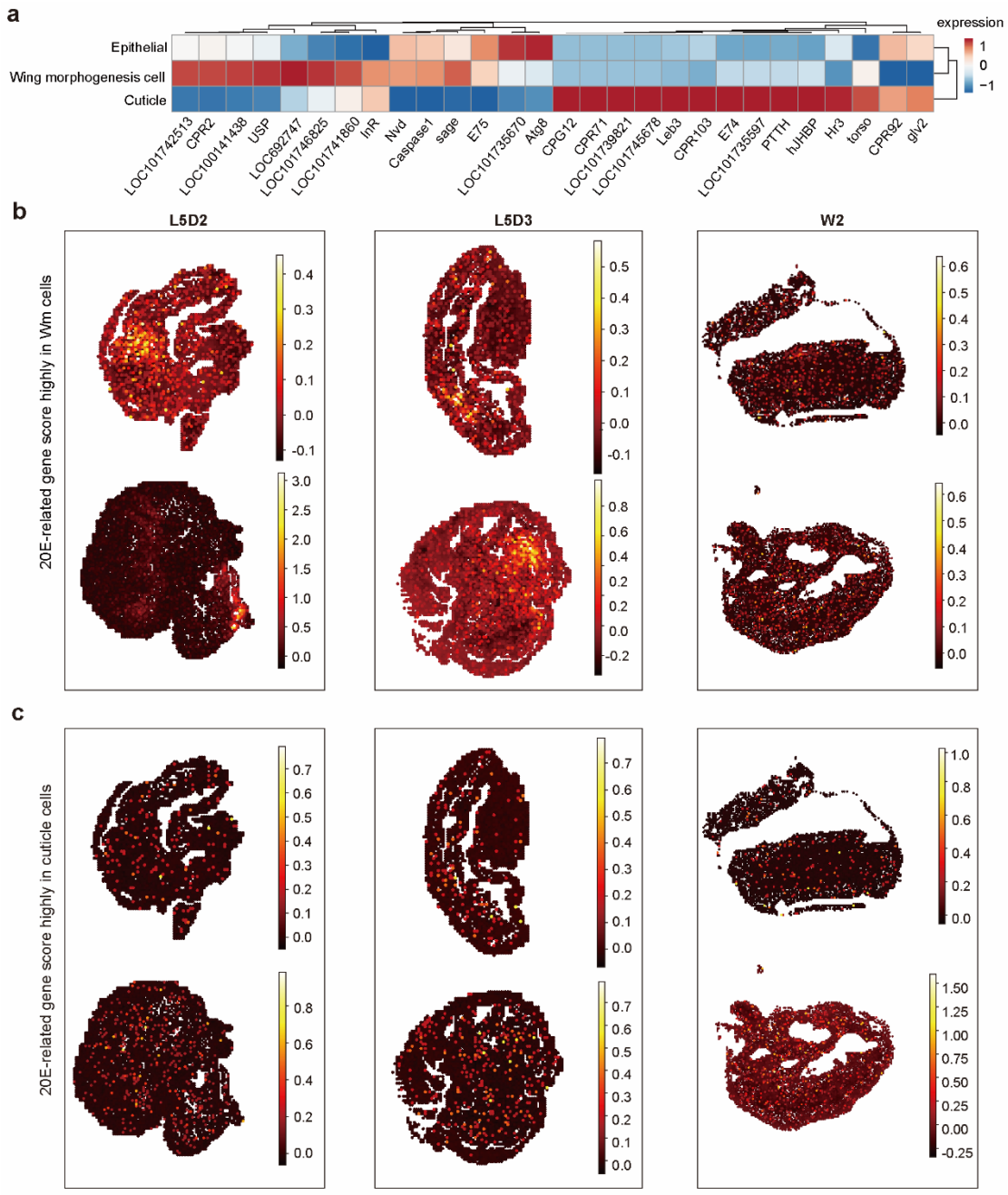

Supplementary Fig. 11. Expression patterns of 20E-related genes in different cell types.

a. Differential expression heatmap of 20E-related genes among three major cell types: epithelial cells, wing morphogenesis cells, and cuticle cells.

b. Spatial visualization of 20E-related gene module scores in Wm cells at three developmental stages (L5D2, L5D3, and W2).

c. Spatial module scores of 20E-related genes in cuticle cells across the same developmental stages.

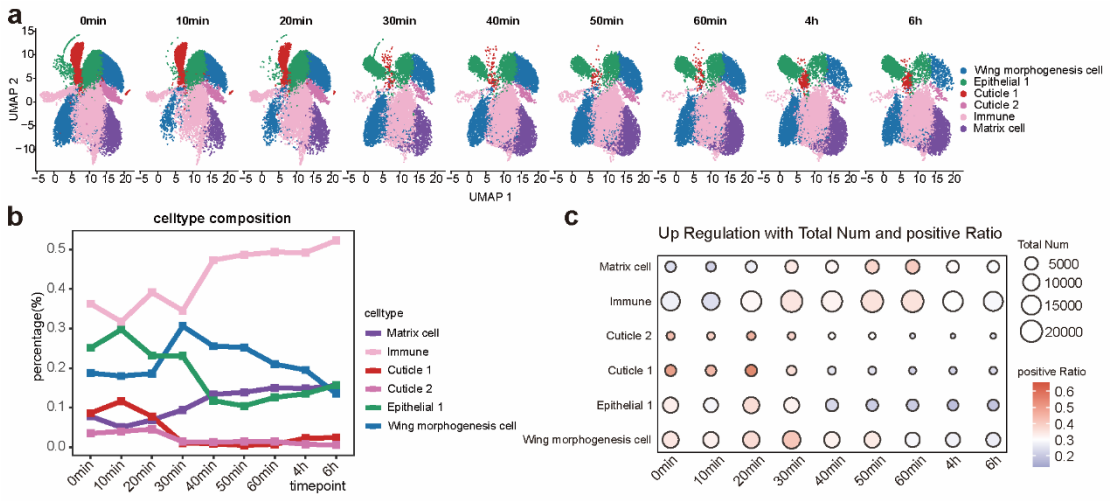

Supplementary Fig. 12. Single-nucleus RNA sequencing (snRNA-seq) analysis of 20E treated wing disc.

a. UMAP plots showing the distribution of different cell types at various time points (0 min–6 h).

b. Temporal changes in the proportions of different cell types.

c. The proportion of time point-specific upregulated genes in different cell types.

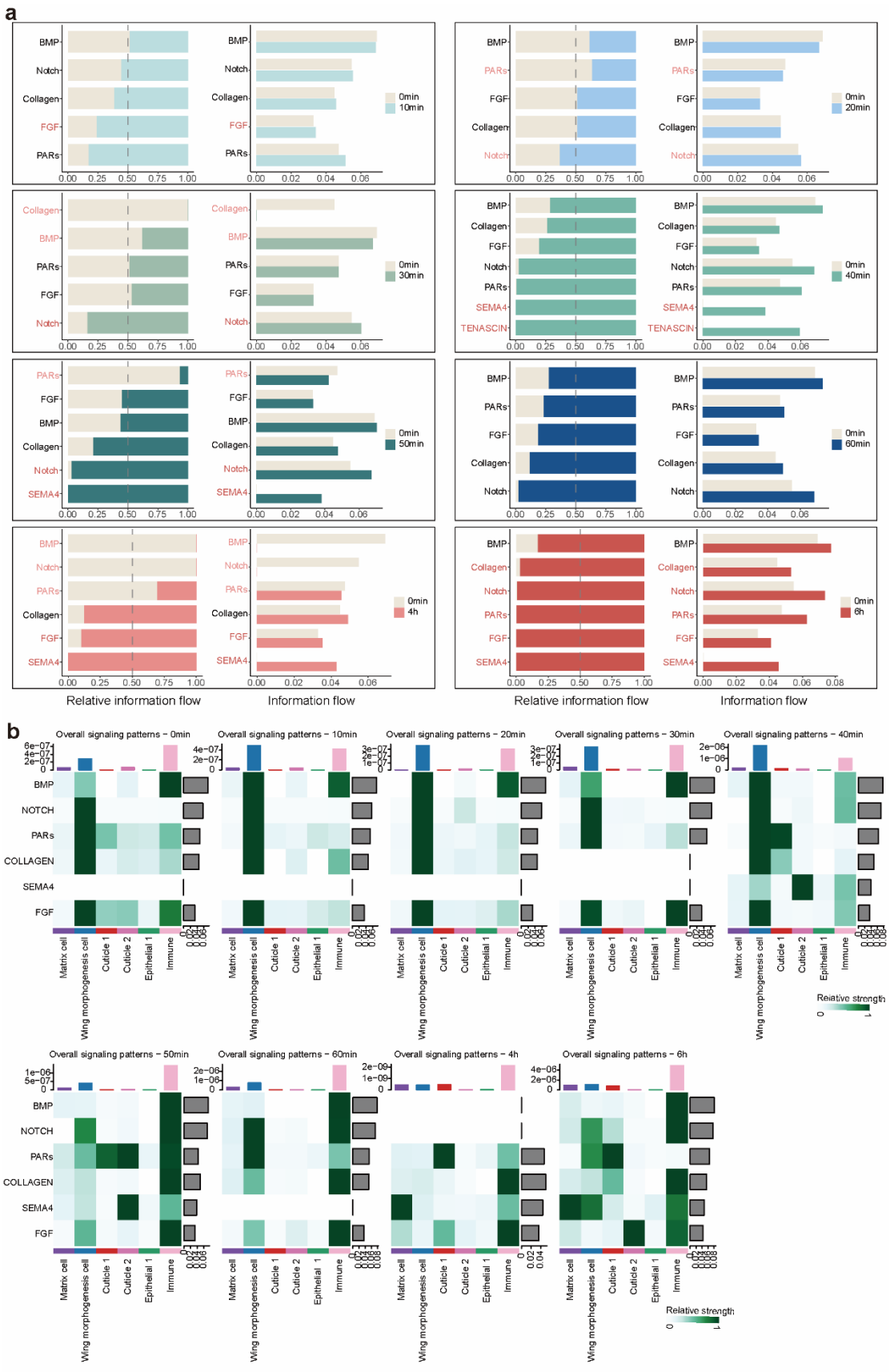

Supplementary Fig. 13. Dynamic signaling pathway activity and intercellular

communication during 20E-induced wing disc development.

a. The relative information flow and information flow of multiple signal pathway networks at different time points (10 min–6 h) as well as at 0 min for the samples are presented. Relative information flow (left) and absolute information flow (right).

b. Temporal dynamics of key signaling pathway activity after 20E treatment.

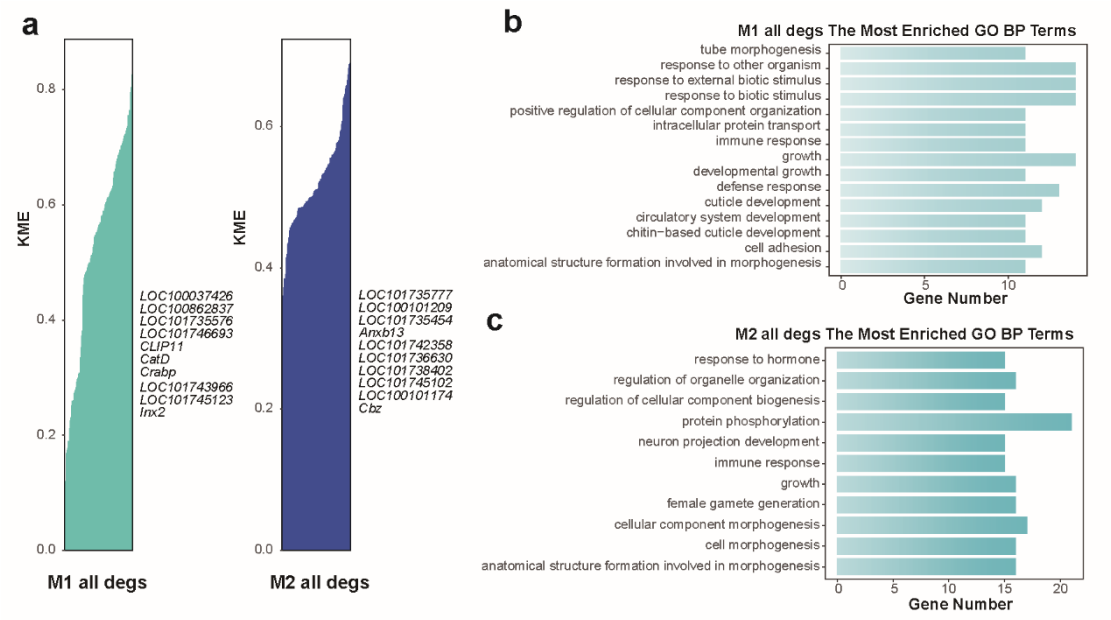

Supplementary Fig. 14. Distinct gene modules before and after 30 min of 20E treatment reveal functional bifurcation.

a. Distribution of KME values for all differentially expressed genes (DEGs) in Modules 1(M1) and 2 (M2).

b. GO Biological Process (BP) enrichment analysis for DEGs in module M1.

c. GO BP enrichment analysis for DEGs in module M2.

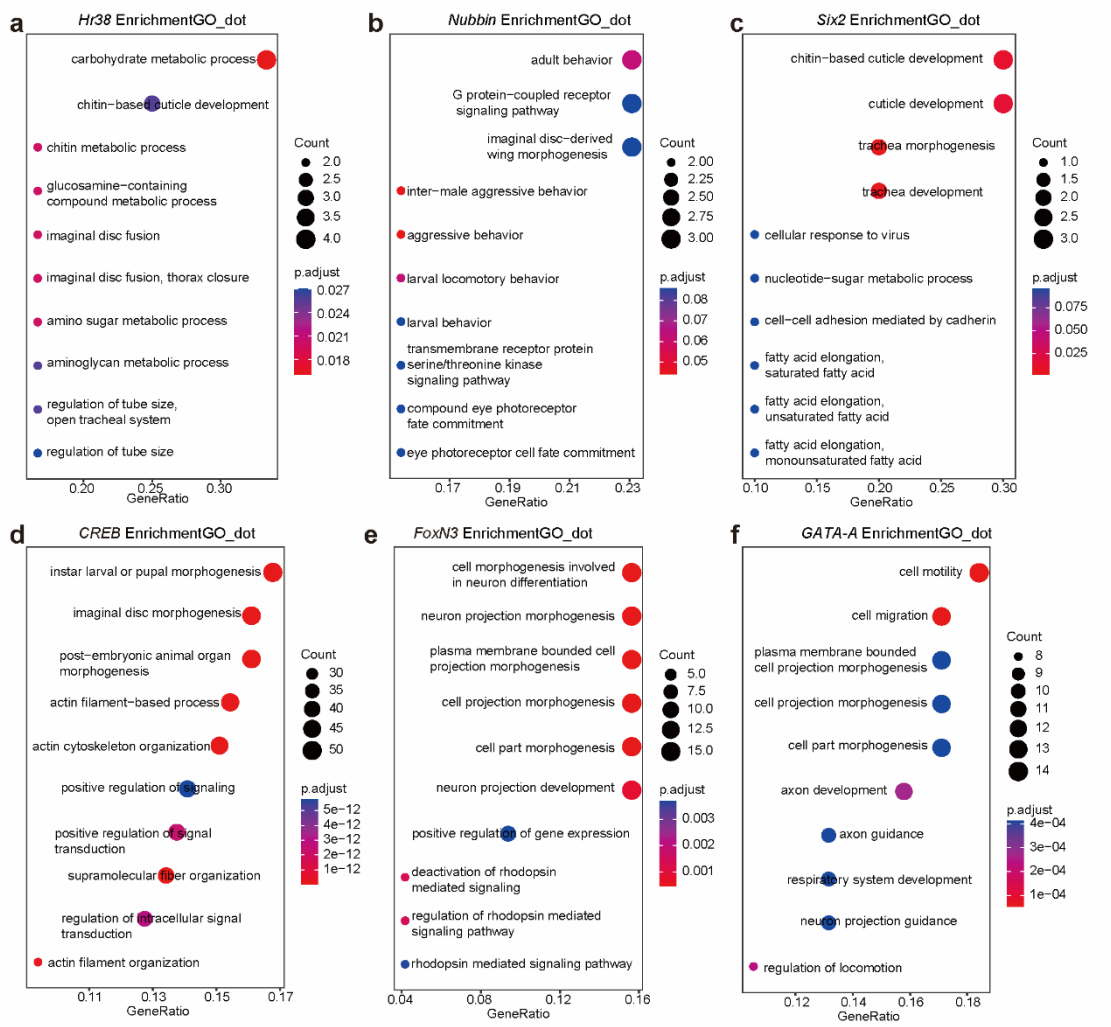

Supplementary Fig. 15. GO enrichment analysis of 20E-responsive Tfs in wing disc.

a–**f**: GO enrichment analysis of six highly expressed TFs after 20E treatment，including *Hr38 (LOC693064), Nubbin (LOC101744796), Six2 (LOC101735990), CREB (LOC692871)*, *FoxN3 (LOC101739133)*, and *GATA-A (LOC10174013).*

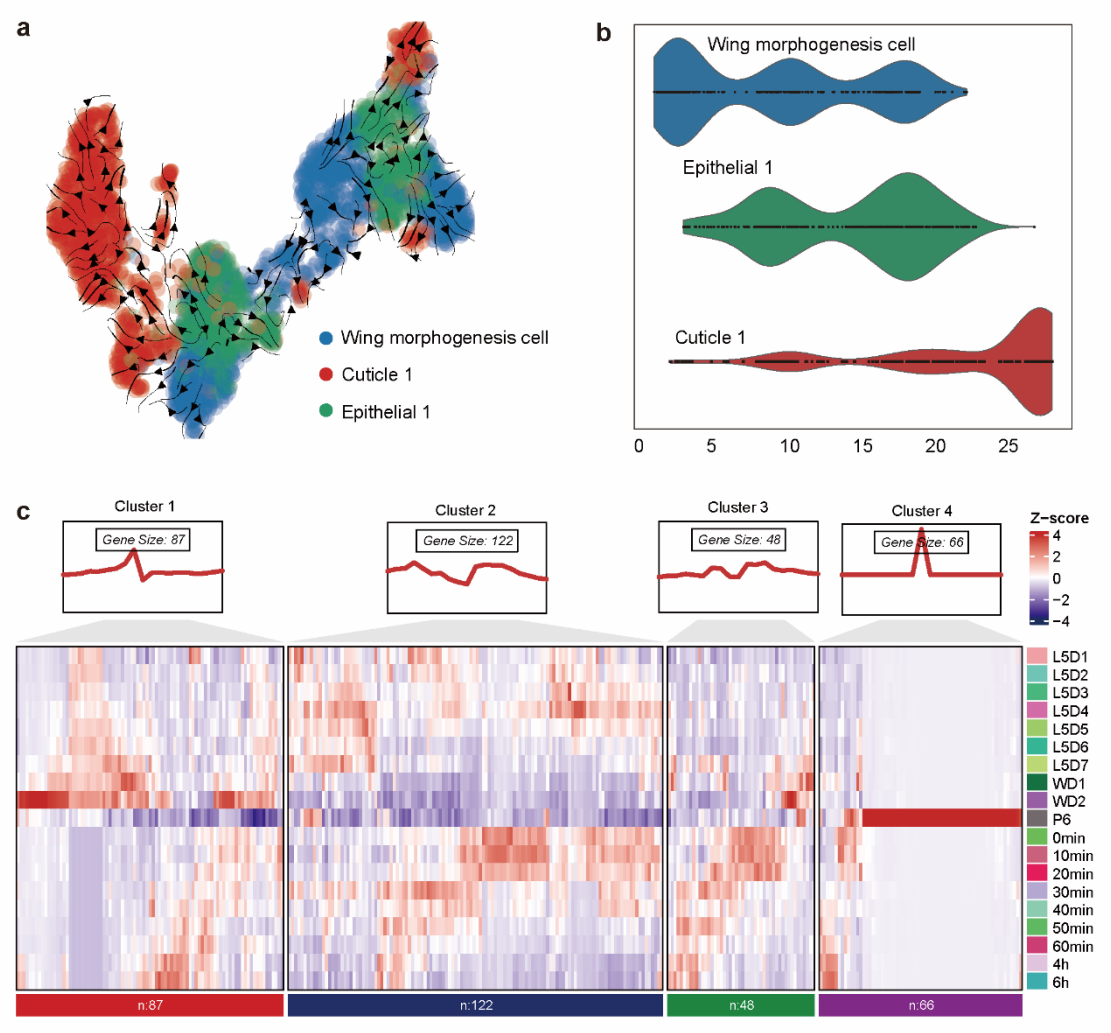

Supplementary Fig. 16. Differentiation trajectory of 20E-treated wing morphogenesis cells.

a. Pseudotime trajectory analysis of Wm cells after 20E treatment.

b. Distribution of three major cell types—Wm cell, Epithelial 1, and Cuticle 1—along pseudotime.

c. Heatmap of the expression dynamics of key regulatory genes involved in Wm transdifferentiation during natural development (L5D1–P6). Their expression was tracked in the 20E-treated group (0–6 h).

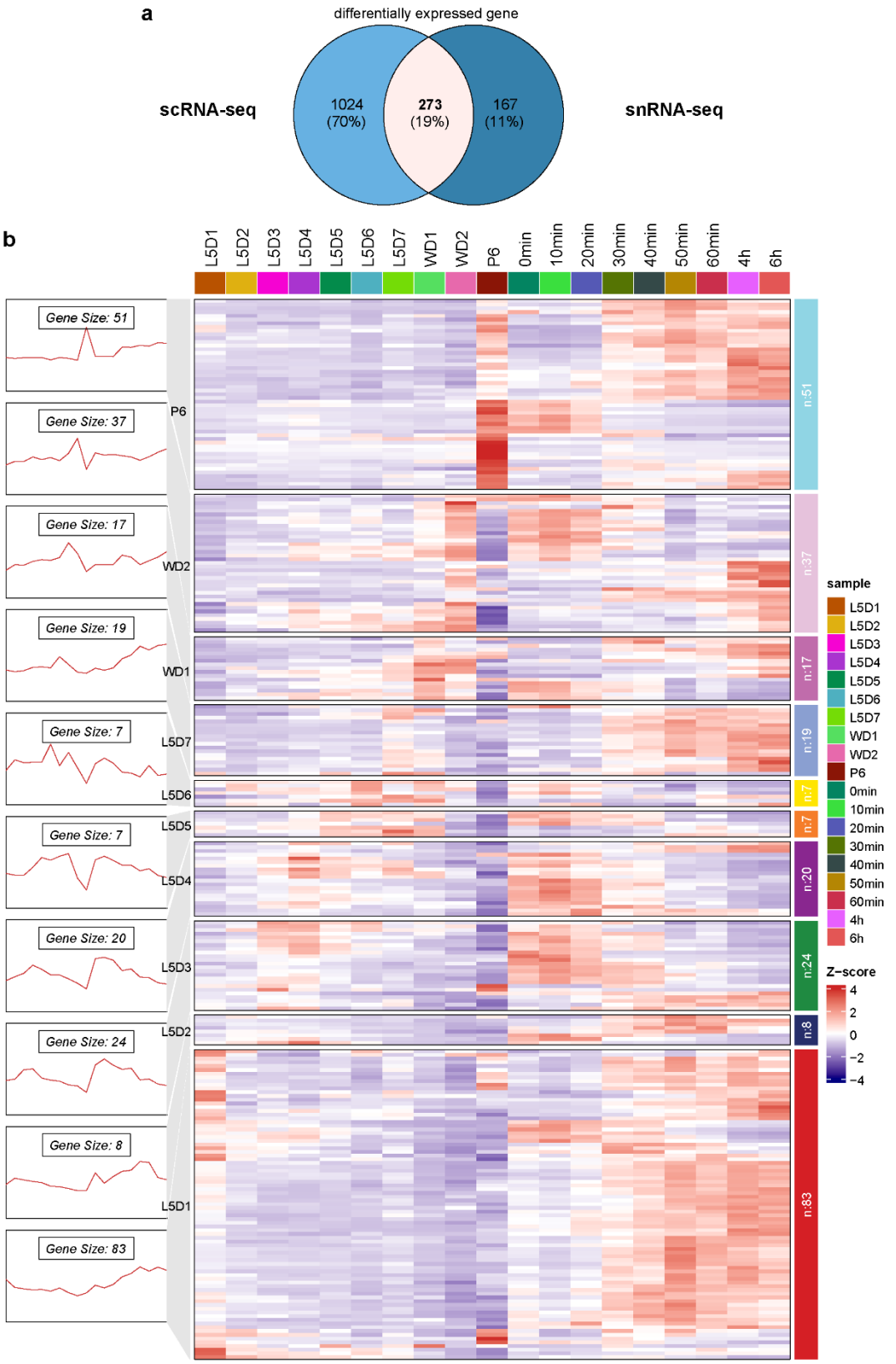

Supplementary Fig. 17. Comparative analysis of DEGs and intersecting genes between scRNA-seq and snRNA-seq datasets.

a. The Venn diagram illustrating the distribution of DEGs in scRNA-seq and

snRNA-seq. Specifically, 167 genes (11%) were exclusively expressed in snRNA-seq, 1024 genes (70%) were exclusively expressed in scRNA-seq, and 273 genes (19%) were expressed in both.

b. Heatmap of the expression profiles of the 273 intersecting DEGs across developmental stages (L5D1–P6) and 20E treatment timepoints (0–6 h).

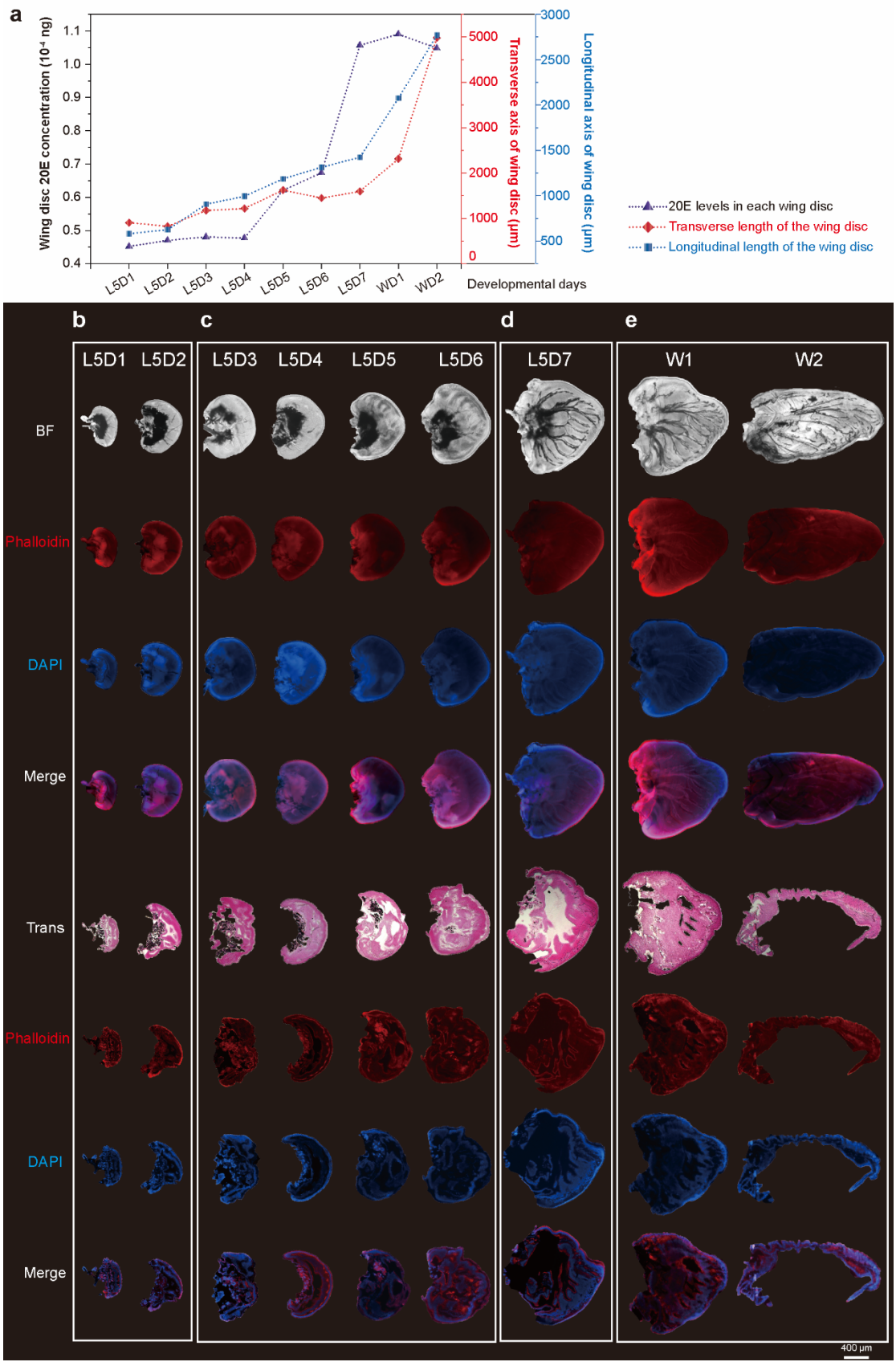

Supplementary Fig. 18. Morphological changes of the wing discs at different developmental stages, visualized using various staining methods.

a. Three *Y*-axes of the correlation between 20E concentration (purple), transverse axis length (red), and longitudinal axis length (blue) of wing disc from L5D1 to W2.

b. During the L5D1 and L5D2 stages of wing primordium development, the wing primordium exhibited a small and smooth morphology.

c. From L5D3 to L5D6 stages of wing primordium development, the wing primordium initiated growth and morphogenesis.

d. At the L5D7 stage of wing primordium development, wing vein structures became distinctly visible, accompanied by the disappearance of sectioned wing bud architecture.

e. During the W1 and W2 stages of wing primordium development, the wing primordium acquired an incipient wing-shaped morphology.

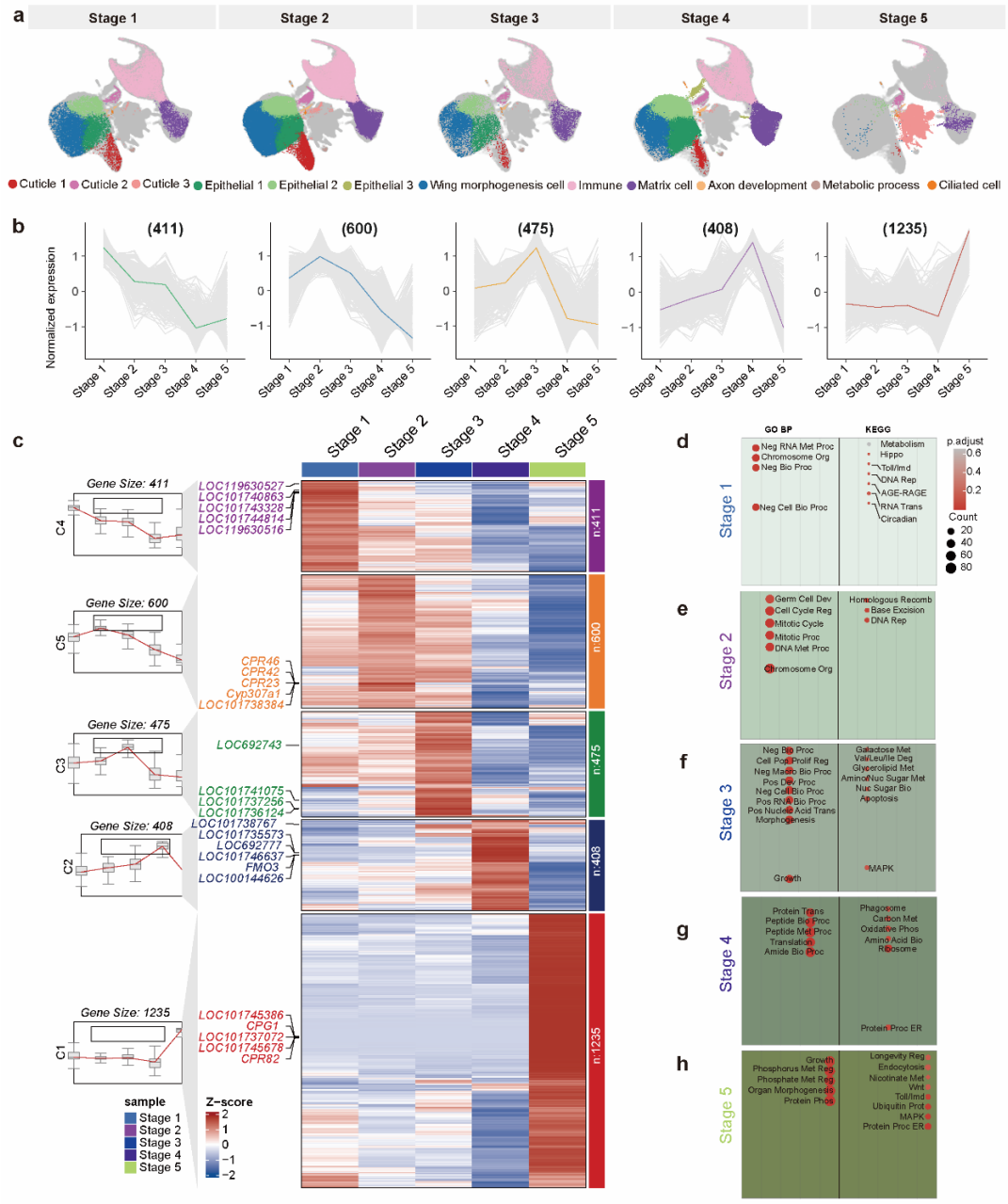

Supplementary Fig. 19. Stage-specific transcriptional programs in wing disc development.

a. UMAP plots showing the dynamic changes in cell types across the five stages.

b. Gene sets enriched in the five developmental stages of the wing discs reflect different key regulatory genes in each stage.

c. Heatmap of DEGs clustered by stage-specific expression patterns.

d–**h**. Summary of KEGG pathway and GO enrichment analysis results for the five different stages. Each stage (Stage 1 to 5) displays significantly enriched biological processes and signaling pathways.

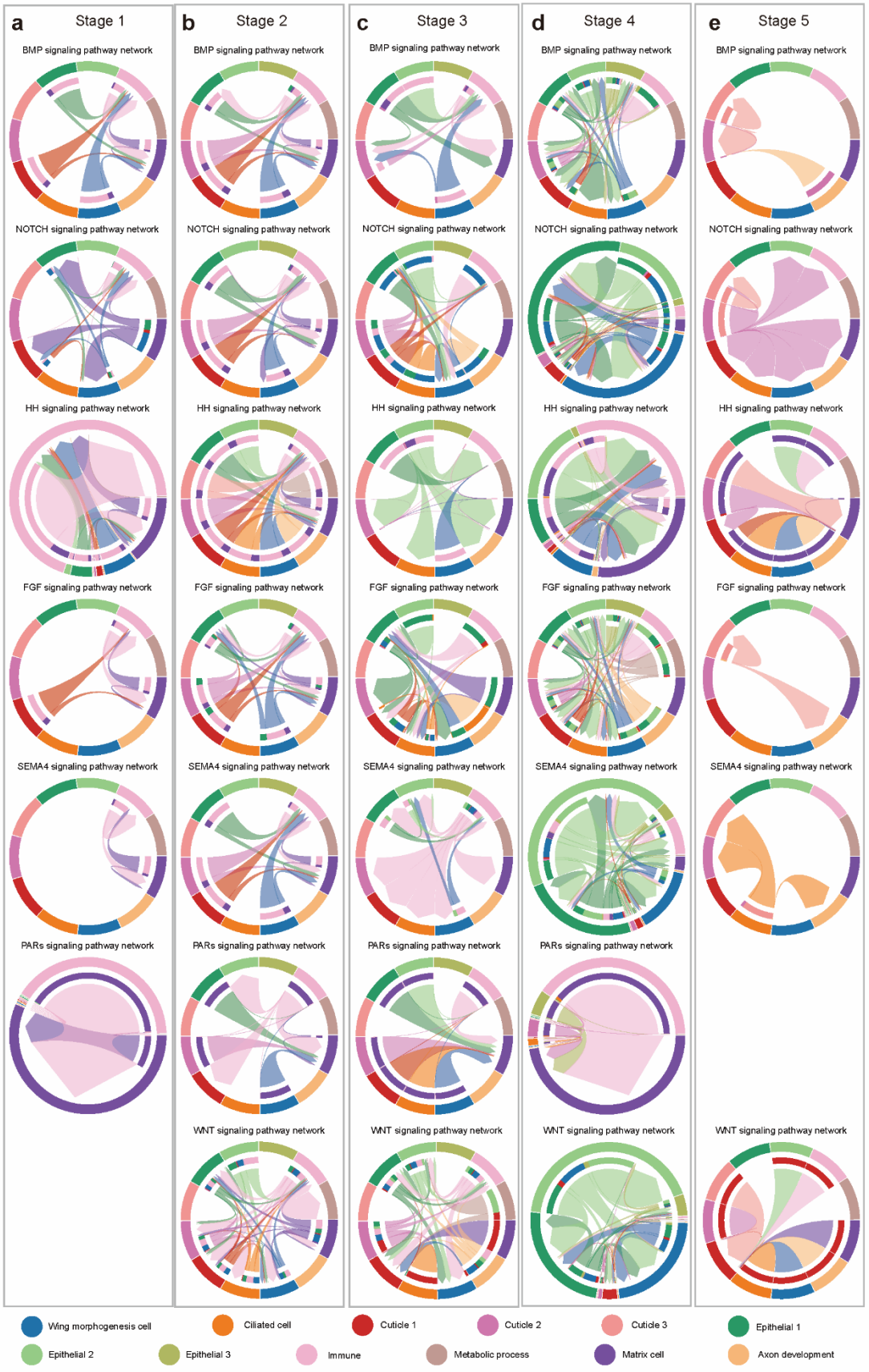

Supplementary Fig. 20. Dynamic cell–cell signaling interactions across five

developmental stages of the wing disc.

a–**e.** Chord diagrams of the intercellular communication networks mediated by key signaling pathways at five developmental stages (Stage 1 to5). Each panel (a–e) corresponds to one developmental stage and includes multiple chord plots representing different pathways. The outer ring is color-coded by cell type, while the inner arcs represent the major interacting cell types. Curved bands connecting the arcs visualize the direction and strength of inferred signaling interactions between cell types.

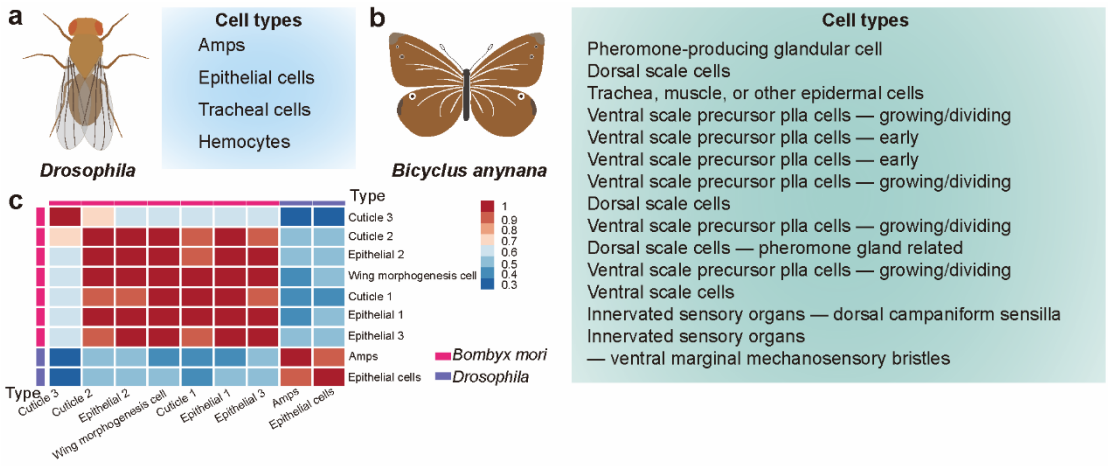

Supplementary Fig. 21. Cross-species comparison of wing disc cell types in *Bombyx mori*, *Drosophila melanogaster*, and *Bicyclus anynana*.

a. Cell types identified in *D melanogaster* wing disc development, including Amps, Epithelial cells, Tracheal cells, and Hemocytes.

b. Cell types identified in *B anynana* wing disc development.

c. Heatmap showing the correlation of cell types between *B mori* and *D melanogaster*.

Reference:

1. Zitnan, D., Sehnal, F. & Bryant, P.J. Neurons producing specific neuropeptides in the central-nervous-system of normal and pupariation-delayed Drosophila. *Developmental Biology* **156**, 117-135 (1993).
2. Rauskolb, C., Correia, T. & Irvine, K.D. Fringe-dependent separation of dorsal and ventral cells in the Drosophila wing. *Nature* **401**, 476-80 (1999).
3. Matsuoka, T. & Fujiwara, H. Expression of ecdysteroid-regulated genes is reduced specifically in the wing discs of the wing-deficient mutant (fl) of Bombyx mori. *Development Genes and Evolution* **210**, 120-128 (2000).
4. Arbouzova, N.I., Bach, E.A. & Zeidler, M.P. Ken & barbie selectively regulates the expression of a subset of Jak/STAT pathway target genes. *Curr Biol* **16**, 80-8 (2006).
5. Zhou, Q.X. *et al.* Analysis of four achaete-scute homologs in Bombyx mori reveals new viewpoints of the evolution and functions of this gene family. *Bmc Genetics* **9**(2008).
6. Nita, M. *et al.* Analysis of ecdysone-pulse responsive region of BMWCP2 in wing disc of Bombyx mori. *Comparative Biochemistry and Physiology B-Biochemistry & Molecular Biology* **153**, 101-108 (2009).
7. Deng, H.M. *et al.* Homeodomain POU and Abd-A proteins regulate the transcription of pupal genes during metamorphosis of the silkworm,. *Proceedings of the National Academy of Sciences of the United States of America* **109**, 12598-12603 (2012).
8. Wang, H.B., Ali, S.M., Moriyama, M., Iwanaga, M. & Kawasaki, H. 20-hydroxyecdysone and juvenile hormone analog prevent precocious metamorphosis in recessive trimolter mutants of. *Insect Biochemistry and Molecular Biology* **42**, 102-108 (2012).
9. LeBon, L., Lee, T.V., Sprinzak, D., Jafar-Nejad, H. & Elowitz, M.B. Fringe proteins modulate Notch-ligand cis and trans interactions to specify signaling states. *Elife* **3**, e02950 (2014).
10. Wang, H.B., Iwanaga, M. & Kawasaki, H. Stage-specific activation of the promoter by low ecdysone concentrations in the wing disc of. *Gene* **537**, 322-327 (2014).
11. Ling, L. *et al.* MiR-2 family targets and to regulate wing morphogenesis in Bombyx mori. *Rna Biology* **12**, 742-748 (2015).
12. Liu, X. *et al.* 20-Hydroxyecdysone (20E) Primary Response Gene E93 Modulates 20E Signaling to Promote Bombyx Larval-Pupal Metamorphosis. *Journal of Biological Chemistry* **290**, 27370-27383 (2015).
13. Liu, S.M. *et al.* Yorkie facilitates organ growth and metamorphosis in Bombyx. *International Journal of Biological Sciences* **12**, 917-930 (2016).
14. Moriyama, M. *et al.* Ecdysteroid promotes cell cycle progression in the Bombyx wing disc through activation of c-Myc. *Insect Biochemistry and Molecular Biology* **70**, 1-9 (2016).
15. Liang, Z. *et al.* Alternative isoforms of BmYki have different transcriptional co-activator activity in the silkworm, Bombyx mori. *International Journal of Biochemistry & Cell Biology* **116**(2019).
16. Wu, S.Y. *et al.* BmBlimp-1 gene encoding a C2H2 zinc finger protein is required for wing development in the silkworm Bombyx mori. *International Journal of Biological Sciences* **15**, 2664-2675 (2019).
17. Xu, J., Yu, Y., Chen, K. & Huang, Y.P. Intersex regulates female external genital and imaginal disc development in the silkworm. *Insect Biochemistry and Molecular Biology* **108**, 1-8 (2019).
18. Yin, J. *et al.* BmSd gene regulates the silkworm wing size by affecting the Hippo pathway. *Insect Science* **27**, 655-664 (2020).
19. Zhang, X.J., Li, D.D., Xu, G.F., Chen, Y.Q. & Zheng, S.C. Signal transducer and activator of transcription is involved in the expression regulation of ecdysteroid-induced insulin-like growth factor-like peptide in the pupal wing

disc of silkworm,. *Insect Science* **27**, 1186-1197 (2020).
20. Wang, Y.P. *et al.* Cytokine receptor DOME controls wing disc development in Bombyx mori. *Insect Biochemistry and Molecular Biology* **148**(2022).
21. Zhang, B. *et al.* The Role of Chitooligosaccharidolytic beta-N-Acetylglucosamindase in the Molting and Wing Development of the Silkworm Bombyx mori. *Int J Mol Sci* **23**(2022).
22. Luo, L., Jian, X. & Sun, H. Cartilage endplate stem cells inhibit intervertebral disc degeneration by releasing exosomes to nucleus pulposus cells to activate Akt/autophagy (vol 39, pg 467, 2021). *Stem Cells* **41**, 415-416 (2023).
23. Qian, W. *et al.* Decapentaplegic retards lipolysis during metamorphosis in Bombyx mori and Drosophila melanogaster. *Insect Biochemistry and Molecular Biology* **155**, 103928 (2023).
24. Everetts, N.J., Worley, M.I., Yasutomi, R., Yosef, N. & Hariharan, I.K. Single-cell transcriptomics of the Drosophila wing disc reveals instructive epithelium-to-myoblast interactions. *Elife* **10**(2021).